COMPUTATIONAL ANALYSIS OF HYDRODYNAMIC EFFECTS IN HYDRAULIC FLOW TURBINES (PART 1)

Viorel BOSTAN

Technical University of Moldova, bd. Stefan cel Mare 168, Chisinau,
viorel_bostan@mail.utm.md

Abstract − **Research and elaboration of the systems for conversion of renewable energy sources (RSE) as a research objective present great interest and importance. Hydraulic energy currently is one of the most used, cheap and clean renewable energy sources. A more efficient use of hydraulic energy, in terms of environmental and social impacts, is the conversion of kinetic energy of running river water without dams' construction. A new design and functional concept of a hydraulic flow turbine with vertical axis and individualized orientation of the hydrodynamic blades was proposed and elaborated. Using a high order panel method the potential flow analysis is performed in order to compute the hydrodynamic lift and moment coefficients. The drag coefficient is computed through a boundary layer analysis. Laminar boundary layer analysis utilizes Falkner-Skan semi-empirical relations. Transition from laminar boundary layer to turbulent boundary layer is predicted through Michael's criterion. The turbulent boundary layer parameters are computed using the Head's model and the drag coefficient is provided by Squire-Young formula. In order to maximize the flowing water energy conversion efficiency the blade hydrodynamic profile parameters and blade orientation with respect to flow direction at each position during the turbine rotation are optimized. The total torque, the forces acting on the blades and the performance of 3-, 4- and 5-blades rotor multi-blade hydrodynamic rotor were analyzed.**

Keywords: *renewable energy sources, hydraulic flow turbine, conversion of hydraulic energy.*

1. INTRODUCTION

The inevitable increase of global energy consumption and the risk of a major environmental impact and climate change as a result of burning fossil fuels open wide prospects for the exploitation of renewable energies. Hydropower, as a renewable energy source, will have an important role in the future. International research confirms that the emission of greenhouse gases is substantially lower in the case of hydropower compared to that generated by burning fossil fuels. From the economical point of view, the utilisation of half of the feasible potential can reduce the emission of greenhouse gases by about 13%; also it can substantially reduce emissions of sulphur dioxide (main cause of acid rains) and nitrogen oxides.

Hydraulic energy is the oldest form of renewable energy used by man and has become one of the most currently used renewable energy sources, being also one of the best, cheap and clean energy sources. Hydraulic energy as a renewable energy source can be captured in two extra power forms:

– potential energy (of the natural water fall);
– kinetic energy (of the water stream running).

Global hydro power energy today is about 715000 MW, or about 19% of global electricity (16% in 2003). However, macro hydro power is not a major option for future energy production for various reasons, such as the environmental one.

Construction of dams on rivers created major environmental and social problems. Development of huge artificial water reservoirs by damming the Earth's major arteries has led to climate and wildlife change in the region, to creating some generating sources of greenhouse gases.

A more efficient use of hydraulic energy, in terms of environmental and social impacts, is the conversion of kinetic energy of running river water without dams' construction. The kinetic energy of water is available continuously. It does not create noise pollution of the environment and doesn't affect aquatic fauna. In the case of small size flow turbines the negative environmental impacts associated with large hydroelectric power stations are also eliminated.

These mini-hydroelectric power stations can meet energy needs of consumers, particularly in remote rural areas.

2. FLOW TURBINE WITH HYDRODYNAMIC EFFECT

The stream velocity of 1m/s represents an energy density of $500W/m^2$ of the flow passage. Still, only part of this energy can be extracted and converted into useful electrical or mechanical energy, depending on the type of rotor and blades. Velocity is important, in particular, since its doubling leads to an 8 times increase of the energy density.

The analysis of the constructive diversion of turbines, proposed previously, does not satisfy completely from the point of view of water kinetic energy conversion efficiency.

Based on the computational analysis of the hydrodynamic effects a hydraulic turbine with vertical axis and hydrofoils with NACA profiles is proposed. The blade orientation with respect to flow direction should be optimized at each position during the turbine rotation.

In order to maximize the flowing water energy conversion efficiency, the selection of the optimal blades hydrodynamic profile is important in flow turbines. Also, conversion increase is achieved by ensuring the optimal position of blades with respect to flow direction at various phases of rotor revolution
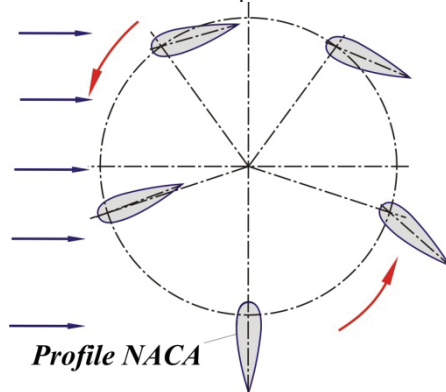

Figure 1: Conceptual scheme of vertical axis turbine with hydrodynamic blades.

(see fig. 1), employing an orientation mechanism of blades. Thus, practically all blades (even those blades which move against the water stream) participate in the generation of the summary torque. Moving in the water flow direction, for torque generation the blades use both the hydrodynamic forces and the water pressure exercised on the blade surfaces. Moving against the water currents direction the blades use only the hydrodynamic lift force for torque generation. Due to the fact that the relative velocity of blades concerning the water currents is twice bigger, practically, at their motion against the water currents, the hydrodynamic lift force is relatively big, and the generated torque is commensurable to the one generated by the water pressure. This effect makes the basis of all patented technical solutions.

3. THEORETICAL JUSTIFICATION OF THE HYDRODYNAMIC PROFILE SELECTION OF THE BLADE

Consider the symmetrical profile of the blade placed in a uniform water stream with velocity $\vec{V}_\infty$ (fig. 2). In the fixing point O' of the symmetrical blade with lever OO' let consider three coordinate systems, namely: the $O'xy$ system with axis $O'y$ oriented in the direction of the velocity vector $\vec{V}_\infty$, and axis $O'x$ normal to this direction; the $O'x'y'$ system with axis $O'y'$ oriented along the lever direction OO', and axis $O'x'$ normal to this direction, and finally the $O'x''y''$

system with axis $O'x''$ oriented along the profile's chord toward the trailing edge and axis $O'y''$ normal to this direction . Points A and B correspond to the trailing and the leading edges, respectively. The angle of attack α is the angle between the profile's chord AB and the direction of the velocity vector $\vec{V}_\infty$, and the positioning angle φ is the angle formed by the velocity vector direction and lever OO'.

The hydrodynamic force $\vec{F}$ has its components in directions $O'x$ and $O'y$, named the lift and drag forces, respectively given by:
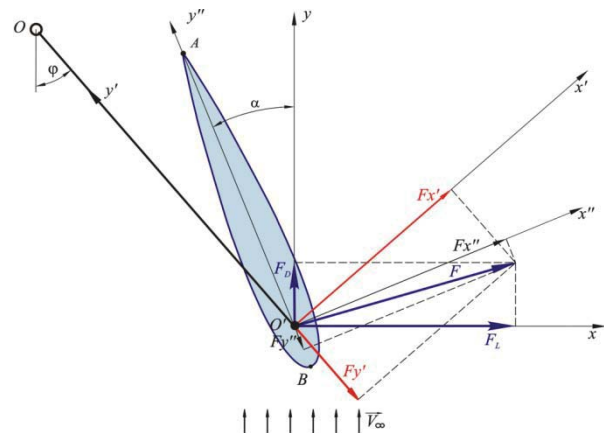

Figure 2: Hydrodynamic profile blade.

$$F_L = \frac{1}{2}C_L\rho V_\infty^2 S_p, \tag{1}$$

$$F_D = \frac{1}{2}C_D\rho V_\infty^2 S_p, \tag{2}$$

where ρ is the fluid density, V_∞ is the flow velocity, $S_p = ch$ (c is the length of chord AB, and h is the blade height) represents the lateral surface area of the blade, and C_L and C_D are dimensionless hydrodynamic coefficients, called the lift coefficient and drag coefficient. The hydrodynamic coefficients C_L and C_D are functions of the angle of attack α, the Reynolds number Re and the hydrodynamic shape of the blade profile. The components of the hydrodynamic force in the coordinate system $O'x'y'$ are

$$\begin{aligned} F_{x'} &= -F_L\sin\varphi + F_D\cos\varphi, \\ F_{y'} &= F_L\cos\varphi + F_D\sin\varphi. \end{aligned} \tag{3}$$

The torque developed by blade i at the rotor spindle OO' is

$$T_{r,i} = F_{x'} \cdot \left| OO' \right|, \tag{4}$$

and the total torque developed by all blades is

$$T_{r\Sigma} = \sum_{i=1}^{Npal} T_{ri}, \tag{5}$$

where $Npal$ is the number of rotor blades.

Generally, the hydrodynamic force does not have application point in the origin of the blade axes system O' so that it produces a resultant moment. The produced moment is determined with respect to a certain reference point. As a reference point there is considered the point located at distance ¼ of the chord length measured from the leading edge B. The moment, called the pitching moment, is computed according to formula

$$M = \frac{1}{2} C_M \rho V_\infty^2 c S_p, \qquad (6)$$

where C_M is the hydrodynamic moment coefficient.

The shape of the hydrodynamic profile is chosen from the library of *NACA* 4 digits aerodynamic profiles. The standard *NACA* 4 digit profiles are characterized by three shape parameters measured in percents of the chord's length: maximum value of camber C_{max}, location of the maximum camber $x_{C,max}$ and maximum thickness G_{max}. The profile coordinates are obtained by combining the camber line and the distribution of thickness [1]. Since the considered blades will have a symmetric shape, the camber is null ($C_{max}=0$, $x_{C,max}=0$) and the camber line will coincide with x-axis.

3.1. Determination of hydrodynamic coefficients C_L and C_M

For simplicity, the profile chord length is considered unitary. Initially, the fluid is considered incompressible and inviscid, and its flow–plane and potential [2,3]. In the case of an incompressible plane potential flow the velocity components $\vec{V} = (u, v)$ in point $P(x,y)$ are given by the relations:

$$u(x, y) = \frac{\partial \Phi}{\partial x}, \quad v(x, y) = \frac{\partial \Phi}{\partial y}, \qquad (7)$$

where potential Φ is obtained by superposition of a uniform velocity flow and a distribution of sources and vortexes on the profile C. Thus, the potential is

$$\Phi = \Phi_\infty + \Phi_S + \Phi_V, \qquad (8)$$

where the uniform flow potential is given by

$$\Phi_\infty = V_\infty x \cos \alpha + V_\infty y \sin \alpha, \qquad (9)$$

the potential of the source distribution with strength $q(s)$ is

$$\Phi_S = \oiint_C \frac{q(s)}{2\pi} \ln(r) ds, \qquad (10)$$

and the potential of vortex distribution with strength $\gamma(s)$ is given by formula:

$$\Phi_V = -\oiint_C \frac{\gamma(s)}{2\pi} \theta ds. \qquad (11)$$

In relations (10, 11) variable s represents the arc length along profile C, and (r, θ) are the polar coordinates of point $P'(x,y)$ relative to the point on the contour corresponding to arc length s (see fig.3).
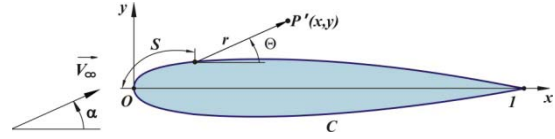

Figure 3: Potential two-dimensional flow around profile C.

Therefore the potential in point $P'(x,y)$ is computed as follows

$$\Phi(P') = V_\infty x \cos \alpha + V_\infty y \sin \alpha$$
$$+ \oiint_C \frac{q(s)}{2\pi} \ln(r) ds - \oiint_C \frac{\gamma(s)}{2\pi} \theta ds. \qquad (12)$$

In order to compute the plane flow potential Φ the collocation method is used, that is: profile C is approximated by a closed polygonal line

$$C \approx \bigcup_{j=1}^{N} E_j,$$

with sides E_j having their vertices P_j and P_{j+1} on C. The vertices P_j are having a higher density near the leading and trailing edges. This is achieved by choosing Chebyshev points as their x-coordinates. Numbering of the vertices starts from the trailing edge on the lower side in the direction of leading edge, passing further to the upper side (fig. 4).
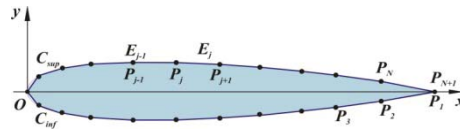

Figure 4: Discretization of profile C.

It is further assumed that the strength of vortexes $\gamma(s)$ distributed on profile C is constant on the boundary having value γ, and the strength of sources $q(s)$ distributed on the profile is piecewise constant on each boundary element E_j with value q_j, $j=1,...,N$. Breaking the integrals in equation (12) along each panel gives:

$$\Phi = V_\infty x \cos \alpha + V_\infty y \sin \alpha$$
$$+ \sum_{j=1}^{N} \int_{E_j} \left(\frac{q_j}{2\pi} \ln(r) - \frac{\gamma}{2\pi} \theta \right) ds \qquad (13)$$

with unknowns γ and q_j, $j = 1, \ldots, N$.

Consider now the boundary element E_j with vertices P_j and P_{j+1}. The unit normal and tangent vectors of the element E_j are given by:

$$n_j = (-\sin \theta_j, \cos \theta_j),$$
$$\tau_j = (\cos \theta_j, \sin \theta_j), \qquad (14)$$

where $\sin\theta_j = \dfrac{y_{j+1} - y_j}{L_j}$ and $\cos\theta_j = \dfrac{x_{j+1} - x_j}{L_j}$.

The unknowns γ and q_j from relation (13) are determined from the boundary and Kutta conditions. The boundary condition is the flow tangency condition along the profile:

$$\vec{V} \cdot \vec{n} = 0, \qquad (15)$$

where $\vec{n}$ is normal to the profile. Imposing condition (15) on collocation points $M_j\left(\bar{x}_j, \bar{y}_j\right)$ chosen to be the midpoints of E_j and denoting the velocity components in M_j by u_j and v_j, respectively, provides N algebraic relations:

$$-u_j \sin\theta_j + v_j \cos\theta_j = 0, \ j = 1, \ldots, N \qquad (16)$$

Relations (16) are used to determine the $N+1$ unknowns: γ and q_j, $j=1,\ldots,N$. The last necessary relation is provided by Kutta condition:

$$\vec{V} \cdot \vec{\tau}\Big|_{E_1} = \vec{V} \cdot \vec{\tau}\Big|_{E_N}, \qquad (17)$$

where $\vec{\tau}$ denotes the unit tangent vector of the boundary element. Kutta condition (17) becomes:

$$u_1 \cos\theta_1 + v_1 \sin\theta_1 = -u_N \cos\theta_N + v_N \sin\theta_N. \quad (18)$$

The velocity components in point M_i are determined by the contributions of velocities induced by the distribution of sources and vortexes on each boundary element E_j:

$$\begin{aligned}
u_i &= V_\infty \cos\alpha + \sum_{j=1}^{N} u_{ij}^s q_j + \sum_{j=1}^{N} u_{ij}^v \gamma, \\
v_i &= V_\infty \sin\alpha + \sum_{j=1}^{N} v_{ij}^s q_j + \sum_{j=1}^{N} v_{ij}^v \gamma,
\end{aligned} \qquad (19)$$

where $u_{ij}^s, v_{ij}^s, u_{ij}^v, v_{ij}^v$ are the influence coefficients.

Let β_{ij}, $i \neq j$, be the angle between $P_j M_i$ and $M_i P_{j+1}$, and set $\beta_{ii} = \pi$. Let $r_{ij} = dist(M_i, P_j)$ and define $D_{ij} = \dfrac{r_{i,j+1}}{r_{ij}}$, $i, j = 1, \ldots, N$. It can be shown that the influence coefficients can be computed by the following formulas:

$$\begin{aligned}
u_{ij}^s &= \frac{1}{2\pi}\left(-\ln D_{ij}\cos\theta_j - \beta_{ij}\sin\theta_j\right), \\
v_{ij}^s &= \frac{1}{2\pi}\left(-\ln D_{ij}\sin\theta_j + \beta_{ij}\cos\theta_j\right), \\
u_{ij}^v &= \frac{1}{2\pi}\left(-\ln D_{ij}\sin\theta_j + \beta_{ij}\cos\theta_j\right), \\
v_{ij}^v &= \frac{1}{2\pi}\left(\ln D_{ij}\cos\theta_j + \beta_{ij}\sin\theta_j\right),
\end{aligned} \qquad (20)$$

Substitute equations (19) and (20) in conditions (16) and (18). After some algebraic manipulations a linear system with $N+1$ equations and $N+1$ unknowns γ and q_j, $j=1,\ldots,N$ is obtained:

$$\left[A_{ij}\right]_{i,j=1}^{N+1}
\begin{bmatrix} q_1 \\ q_2 \\ \vdots \\ q_N \\ \gamma \end{bmatrix}
=
\begin{bmatrix} b_1 \\ b_2 \\ \vdots \\ b_N \\ b_{N+1} \end{bmatrix}. \qquad (21)$$

Coefficients A_{ij} and b_i are given by formulas:

$$A_{ij} = \frac{1}{2\pi}\left(\sin\Delta_{ij}\ln D_{ij} + \beta_{ij}\cos\Delta_{ij}\right), \ i,j = 1,\ldots,N,$$

$$A_{i,N+1} = \frac{1}{2\pi}\sum_{j=1}^{N}\left(\cos\Delta_{ij}\ln D_{ij} - \beta_{ij}\sin\Delta_{ij}\right), \ i = 1,\ldots,N,$$

$$\begin{aligned}
A_{N+1,j} = \frac{1}{2\pi}\Big(&\beta_{1,j}\sin\Delta_{1j} + \beta_{N,j}\sin\Delta_{Nj} \\
&-\cos\Delta_{1j}\ln D_{1j} - \cos\Delta_{Nj}\ln D_{N,j}\Big),
\end{aligned}$$

$$\begin{aligned}
A_{N+1,N+1} = \frac{1}{2\pi}\sum_{j=1}^{N}\Big(&\sin\Delta_{1j}\ln D_{1j} + \sin\Delta_{Nj}\ln D_{N,j} \\
&+\beta_{1j}\cos\Delta_{1j} + \beta_{Nj}\cos\Delta_{Nj}\Big),
\end{aligned}$$

$$b_i = V_\infty \sin\left(\theta_i - \alpha\right), \ i = 1,\ldots,N,$$

$$b_{N+1} = -V_\infty \cos(\theta_1 - \alpha) - V_\infty \sin(\theta_N - \alpha)$$

with $\Delta_{ij} = \theta_i - \theta_j$.

The solution of linear system (21) will provide the values of γ and q_j, $j=1,\ldots,N$, using which the tangential components of the velocity in collocation points M_i, $i=1,\ldots,N$ can be computed. The tangential component of the velocity at point M_i is

$$u_{\tau i} = u_i \cos\theta_i + v_i \sin\theta_i.$$

Substitute (19) in the above relation to obtain:

$$\begin{aligned}
u_{\tau i} = &\left(V_\infty \cos\alpha + \sum_{j=1}^{N} u_{ij}^s q_j + \sum_{j=1}^{N} u_{ij}^v \gamma\right)\cos\theta_i \\
&+ \left(V_\infty \sin\alpha + \sum_{j=1}^{N} v_{ij}^s q_j + \sum_{i=1}^{N} v_{ij}^v \gamma\right)\sin\theta_i.
\end{aligned}$$

Using relations (20) and algebraic manipulations obtain the following formulas:

$$\begin{aligned}
u_{\tau i} = &\cos\left(\theta_i - \alpha\right)V_\infty \\
&+ \frac{1}{2\pi}\sum_{j=1}^{N}\Big(q_i\left(\beta_{ij}\sin\Delta_{ij} - \cos\Delta_{ij}\ln D_{ij}\right) \qquad (22) \\
&+\gamma\left(\sin\Delta_{ij}\ln D_{ij} - \beta_{ij}\cos\Delta_{ij}\right)\Big).
\end{aligned}$$

The local pressure coefficient can be rewritten as

$$C_p = 1 - \frac{V^2}{V_\infty^2}.$$

Therefore, the local pressure coefficient on the discretized profile can be computed from the relation

$$C_{p,i} = 1 - \left(\frac{u_{\tau i}}{V_\infty} \right)^2, \qquad (23)$$

where $u_{\tau i}$ are given by (22). The hydrodynamic forces acting on the boundary element E_j are given by:

$$\begin{aligned} f_{xj} &= C_{p,j} \left(y_{j+1} - y_j \right), \\ f_{yj} &= C_{p,j} \left(x_{j+1} - x_j \right), \end{aligned} \qquad (24)$$

and the pitching moment coefficient is calculated by:

$$c_{m,j} = -f_{xj} \left(\frac{y_{j+1} - y_j}{2} \right) + f_{yj} \left(\frac{x_{j+1} - x_j}{2} - \frac{c}{4} \right). \quad (25)$$

The total force is the sum of contributions of each boundary element:

$$F_x = \sum_{j=1}^{N} f_{xj}, \quad F_y = \sum_{j=1}^{N} f_{yj}, \qquad (26)$$

Lift and moment coefficients are given by:

$$C_L = -F_x \sin\alpha + F_y \cos\alpha, \qquad (27)$$

$$C_M = \sum_{j=1}^{N} c_{m,j}. \qquad (28)$$

3.2. Determination of hydrodynamic drag coefficient C_D

The first phase, described in previous section, consists in the computation of the velocity distribution in the potential flow around the profile. The next phase consists in the computation of boundary layer parameters corresponding to the velocity distribution obtained in the first phase. In its turn, the boundary layer phase is divided into two sub-steps: laminar boundary layer and turbulent boundary layer [4-6].

The boundary layer starts at the stagnation point (the point on the profile's contour with zero velocity) and follows the profile along the upper or lower surface in the direction of trailing edge. As soon as the stagnation point x_1 was determined, the numbering of vertices starts in the direction of trailing edge (fig.5).
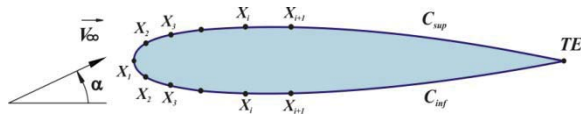

Figure 5: Profile discretization for boundary layer analysis.

The computation of laminar boundary layer parameters is based on the integral momentum and kinetic energy equations. The boundary layer thickness is defined as the distance from the profile at which the flow velocity differs by 1% from the velocity corresponding to the potential flow. Prandtl laminar boundary layer equations are derived from the steady incompressible Navier-Stokes equations:

$$\frac{\partial u}{\partial x} + \frac{\partial v}{\partial y} = 0,$$

$$\rho \left(u \frac{\partial u}{\partial x} + v \frac{\partial v}{\partial y} \right) = -\frac{\partial p}{\partial x} + \mu \frac{\partial^2 u}{\partial y^2}, \qquad (29)$$

$$\frac{\partial p}{\partial y} = 0.$$

Here, x represents the measured distance along the contour from the stagnation point, and y is the measured distance in the normal to the surface direction (fig. 6).
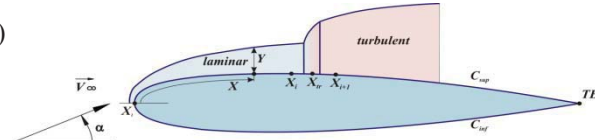

Figure 6: Transition from laminar to turbulent boundary layer.

Introduce the displacement thickness δ^*:

$$\delta^* = \int_0^\infty \left(1 - \frac{u}{V} \right) dy, \qquad (30)$$

where V represents the velocity of the boundary layer exterior part in the considered point, and u is the tangential velocity in this point. Similarly, the momentum thickness θ is defined by

$$\theta = \int_0^\infty \left(1 - \frac{u}{V} \right) \frac{u}{V} \, dy, \qquad (31)$$

and the kinetic energy thickness θ^* is given by

$$\theta^* = \int_0^\infty \left(1 - \frac{u^2}{V^2} \right) \frac{u}{V} dy. \qquad (32)$$

By integrating equations (29) and using relations (30−32), the Von Karman integral-differential momentum equation is obtained

$$\frac{d\theta}{dx} + \frac{\theta}{V} \left(2 + \frac{\delta^*}{\theta} \right) \frac{dV}{dx} = \frac{1}{2} C_f, \qquad (33)$$

where C_f denotes the local friction coefficient on the profile surface. Introduce the shape parameter

$$H = \frac{\delta^*}{\theta}. \qquad (34)$$

Then, equation (33) can be rewritten as follows:

$$\frac{d\theta}{dx} + (2+H)\frac{\theta}{V}\frac{dV}{dx} = \frac{1}{2}C_f. \qquad (35)$$

On the other side, multiply equation (33) by u, and integrate it in order to obtain:

$$\frac{d\theta^*}{dx} + 3\frac{\theta^*}{V}\frac{dV}{dx} = 2C_d, \qquad (36)$$

where C_d is the dissipation coefficient. Introduce the second shape parameter:

$$H^* = \frac{\theta^*}{\theta}. \qquad (37)$$

Subtract equation (35) from equation (36) to get:

$$\theta\frac{dH^*}{dx} + H^*(H-1)\frac{\theta}{V}\frac{dV}{dx} = 2C_d - \frac{1}{2}H^*C_f. \quad (38)$$

The system of equations (35) and (38) is not sufficient to determine all unknowns. The additional relations are based on Falkner-Skan semi-empirical relations [5]. Assume the following correlation between H^* and H:

$$H^* = \begin{cases} 0.076\dfrac{(H-4)^2}{H}+1.515, & \text{if } H < 4, \\[2mm] 0.04\dfrac{(H-4)^2}{H}+1.515, & \text{otherwise.} \end{cases} \qquad (39)$$

Also let $\mathrm{Re}_\theta = \mathrm{Re}\cdot\theta\cdot V$ and assume that

$$\frac{1}{2}\mathrm{Re}_\theta\, C_f = F_1(H), \quad 2\mathrm{Re}_\theta\frac{C_d}{H^*} = F_2(H),$$

where

$$F_1(H) = \begin{cases} 0.01977\dfrac{(H-7.4)^2}{H-1}-0.067, & \text{if } H < 7.4, \\[2mm] 0.022\dfrac{(H-7.4)^2}{(H-6)^2}-0.067, & \text{otherwise,} \end{cases} \qquad (40)$$

$$F_2(H) = \begin{cases} 0.00205(4-H)^{11/2}+0.207, & \text{if } H < 4, \\[2mm] \dfrac{-0.003(H-4)^2}{1+0.02(H-4)^2}+0.207, & \text{otherwise.} \end{cases} \qquad (41)$$

Multiply equation (35) by Re_θ and let $\omega = (\mathrm{Re}_\theta)^2$. The terms are re-arranged to obtain:

$$\frac{1}{2}V\frac{d\omega}{dx} + (2+H)\omega\frac{dV}{dx} = F_1(H). \qquad (42)$$

Multiply equation (38) by Re_θ/H^* and re-arrange terms to get:

$$\omega V\frac{d(\ln H^*)}{dH}\frac{dH}{dx} + (1-H)\omega\frac{dV}{dx} = F_2(H)-F_1(H). \quad (43)$$

Introduce the following notations:

$$A(x) = \frac{dV}{dx}, \quad F_3(H) = \frac{d(\ln H^*)}{dH},$$
$$F_4(H) = F_2(H)-F_1(H).$$

Then equations (42) and (43) are rewritten as follows

$$\frac{1}{2}V(x)\frac{d\omega}{dx} + (2+H)\omega A(x) = F_1(H),$$
$$\omega V(x)F_3(H)\frac{dH}{dx} + (1-H)\omega A(x) = F_4(H). \qquad (44)$$

The initial values are chosen to ensure that

$$\frac{dw}{dx}(0) = 0 \text{ and } \frac{dH}{dx}(0) = 0.$$

Therefore, $H(0)$ is the solution of the following equation:

$$\frac{1-H}{2+H} = \frac{F_4(H)}{F_1(H)}.$$

Solving the above equation provides us the root $H(0) \approx 2.24$. Consequently,

$$\omega(0) = \frac{F_1(H(0))}{A(0)(2+H(0))}.$$

The initial conditions become

$$w(0) = \frac{F_1(2.24)}{4.24\,A(0)},$$
$$H(0) = 2.24. \qquad (45)$$

The system of nonlinear ODE (44) with initial conditions (45) is solved by the Backward Euler method, but in order to avoid the implicit iterations at the transition from step j to step $j+1$ the functions F_1 and F_4 are linearized in the neighborhood of H_j, while F_3 takes the value $F_3(H_j)$. Thus, there is obtained a system of two bilinear equations with the unknowns H_{j+1} and ω_{j+1}:

$$A_j^1\omega_{j+1} + B_j^1 H_{j+1}\omega_{j+1} + C_j^1 H_{j+1} = D_j^1,$$
$$A_j^2\omega_{j+1} + B_j^2 H_{j+1}\omega_{j+1} + C_j^2 H_{j+1} = D_j^2, \qquad (46)$$

where

$$A_j^1 = \frac{V(x_{j+1})}{2\Delta x} + 2A(x_{j+1}),$$
$$B_j^1 = A(x_{j+1}),$$
$$C_j^1 = -F_1'(x_j),$$
$$D_j^1 = \frac{V(x_{j+1})}{2\Delta x}\omega_j + F_1(x_j) - F_1'(x_j)H_j = 0,$$
$$A_j^2 = A(x_{j+1}) - \frac{F_3(x_j)H_j V(x_{j+1})}{\Delta x},$$

$$B_j^2 = \frac{F_3(x_j)V(x_{j+1})}{\Delta x} - A(x_{j+1}),$$

$$C_j^2 = -F_4'(x_j),$$

$$D_j^1 = F_4(x_j) - F_4'(x_j)H_j.$$

This method is iterated till either the transition from the laminar layer to the turbulent layer is predicted (transition point x_{tr}, fig. 6) or till the trailing edge *TE* is reached.

In order to locate the transition from laminar boundary layer to turbulent boundary layer the Michel criterion is being used [7]. Let $\mathrm{Re}_x = \mathrm{Re}\,Vx$ and

$$\mathrm{Re}_{\theta\max} = 1.174\left(1 + \frac{22.4}{\mathrm{Re}_x}\right)\mathrm{Re}_x^{0.46}. \qquad (47)$$

Then, transition takes place if $\mathrm{Re}_\theta > \mathrm{Re}_{\theta\max}$. Transition point is the root of the linear interpolation of $\mathrm{Re}_\theta(x) - \mathrm{Re}_{\theta\max}(x)$.

To analyze the turbulent boundary layer introduce the mean values and fluctuations:

$$\overline{q}(x,y) = \lim_{T\to\infty} \frac{1}{T} \int_{t_0}^{t_0+T} q(x,y,t)dt, \qquad (48)$$

$$q'(x,y,t) = q(x,y,t) - \overline{q}(x,y). \qquad (49)$$

The equations of the turbulent boundary layer are obtained from the Navier-Stokes equations:

$$\frac{\partial \overline{u}}{\partial x} + \frac{\partial \overline{v}}{\partial y} = 0,$$

$$\rho\left(\overline{u}\frac{\partial \overline{u}}{\partial x} + \overline{v}\frac{\partial \overline{u}}{\partial y}\right) = -\frac{\partial \overline{p}}{\partial x} + \frac{\partial}{\partial y}\left(\mu\frac{\partial \overline{u}}{\partial y} - \rho\overline{u'v'}\right), \quad (50)$$

$$\frac{\partial \overline{p}}{\partial y} = \frac{\partial}{\partial y}\left(\mu\frac{\partial \overline{v}}{\partial y} - \rho\overline{v'^2}\right).$$

Similarly to the case of laminar boundary layer, the Von Karman integral equations are obtained. The computations of the turbulent boundary layer parameters are done by applying the Head's model [6]. Consider the flow volume in the boundary layer at an arbitrary point x:

$$Q(x) = \int_0^{\delta(x)} udy.$$

Then the displacement thickness is given by:

$$\delta^* = \delta - \frac{Q}{V}.$$

Introduce the entrainment velocity:

$$E = \frac{dQ}{dx},$$

that can be rewritten as

$$E = \frac{d}{dx}(V\theta H_1),$$

where

$$H_1 = \frac{\delta - \delta^*}{\theta}.$$

According to the Head's model the dimensionless velocity E/V depends only on H_1, and H_1, in its turn, depends only on H. Cebeci and Bradshow [5] have considered the empirical relations

$$\frac{E}{V} = 0.0306(H_1 - 3)^{-0.6169} \qquad (51)$$

And consequently

$$H_1 = \begin{cases} 0.8234(H-1.1)^{-1.287} + 3.3, & H \le 1.6, \\ 1.5501(H-0.6778)^{-3.064} + 3.3, & \text{otherwise.} \end{cases} \quad (52)$$

Finally, the last equation to determine the unknowns θ, H, H_1 and C_f is the Ludwieg-Tillman wall friction law:

$$C_f = \frac{0.246}{10^{0.678H}\,\mathrm{Re}_\theta^{0.268}}. \qquad (53)$$

Combine the Von Karman integral equation and the relations (51)−(53) to obtain the following ODE system:

$$\frac{dY}{dx} = g(Y,x), \qquad (54)$$

where $Y = \begin{bmatrix} \theta & H_1 \end{bmatrix}^T$, and

$$g(Y,x) = \begin{bmatrix} -\dfrac{\theta(H_1+2)}{V}\dfrac{dV}{dx} + \dfrac{1}{2}C_f \\[2mm] -\dfrac{H_1}{V}\dfrac{dV}{dx} - \dfrac{H_1}{\theta}\dfrac{d\theta}{dx} + \dfrac{0.0306}{\theta(H_1-3)^{0.6169}} \end{bmatrix}.$$

The initial values are the final values supplied by the laminar boundary layer step. The numerical integration of system (54) is done by Runge-Kutta method of order 2, namely:

$$Y^* = Y_j + h_j g(Y_j, x_j),$$

$$Y_{j+1} = Y_j + h_j\left(\frac{1}{2}g(Y_j, x_j) + \frac{1}{2}g(Y^*, x_j)\right).$$

The calculation is done either till the trailing edge is reached or till the separation of the turbulent layer occurs.

Squire-Young formula [8] is applied to compute the drag coefficient C_D:

$$C_D = 2\left(\theta V^\lambda\big|_{x_{TE},C_{upper}} + \theta V^\lambda\big|_{x_{TE},C_{lower}}\right), \qquad (55)$$

where $\lambda = \left(H\big|_{x_{TE}} + 5\right)\big/2$.

3.3. Selection of the optimal hydrodynamic profile of blades

The optimization of the performance of the turbine with hydrodynamic blades demands an optimal hydrodynamic profile of the blade. The numerical methods, described previously, are used to compute the hydrodynamic coefficients $C_{L,ref}$ and $C_{D,ref}$ for the symmetrical profiles selected from the *NACA* library of aerodynamic profiles with a reference chord length $c_{ref}=1m$. Fig. 7 shows the hydrodynamic lift $C_{L,ref}$ and drag $C_{D,ref}$ coefficients. Taking into account the data from Fig. 7, the *NACA 0016* hydrodynamic profile is being selected as the reference profile.
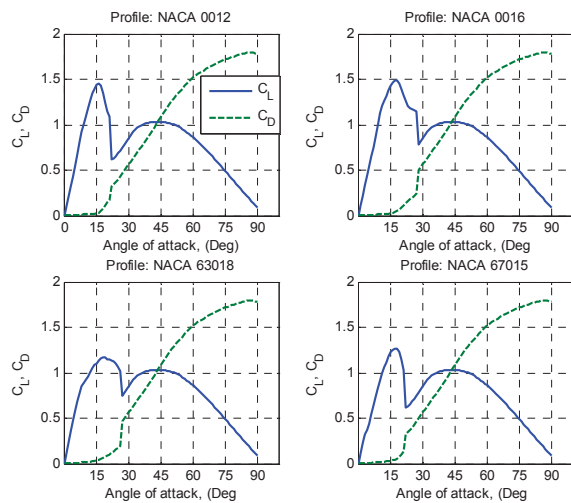
Figure 7: Hydrodynamic lift C_L and drag C_D coefficients versus the angle of attack for NACA 0012, 0016, 63018 and 67015 profiles.

4. THE TORQUE AND THE FORCES ACTING ON THE MULTI-BLADE HYDRAULIC TURBINE

The numerical methods, described previously, are used to compute the hydrodynamic coefficients corresponding to NACA 0016 profile with the chord length $c_{ref} = 1\ m$: $C_{L,ref}, C_{M,ref}$ and $C_{D,ref}$ by formulas (27), (28) and (55). The coefficients corresponding to the profile with the chord length *1.3 m* are calculated from the relations:

$$C_L = 1.3 C_{L,ref},$$
$$C_M = (1.3)^2 C_{M,ref}, \qquad (56)$$
$$C_D = 1.3 C_{D,ref}.$$

The working angle of attack is selected to be $\alpha = 18^o$. During a full revolution around the rotor's axis the blade changes its attack angle depending on its position (fig. 8). Thus, in sector I the angle of attack (angle formed by the blade's chord and water flow direction) is 18°; in sector II the angle of attack shifts

from 18° up to -18°, but the blade does not contribute to the total torque developed at the rotor shaft. In this sector, extended up to approximately 60°, the blade is carried freely by the water flow and its re-positioning ends with an angle of attack of -18° at the end of sector III. The angle of attack is -18° in sector III. In sectors IV-VI the hydrodynamic effect is minimal and the blade has to be re-positioned from angle -18° to angle 18. In order to use the kinetic energy in the sectors IV-VI it is proposed to re-position the blade from -18° to 90° in sector IV; in sector V the blade remains under an angle of 90°, and in sector VI the angle of attack returns to 18°. Knowing the values of the hydrodynamic coefficients C_L and C_D, the lift force F_L and drag force F_D are computed using relations (1) and (2), and relation (3) supplies the normal and tangential components of the hydrodynamic force.
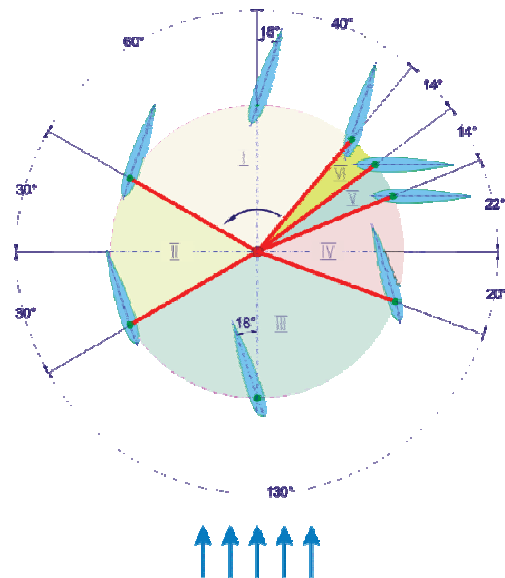

Figure 8: Blade position and working areas.

The magnitude of the hydrodynamic force $\vec{F}$ acting on the blade, and its tangential and normal components F_x and F_y versus the positioning angle are presented in fig. 9. The following constructive parameters of the rotor were considered: rotor radius $R = 2m$, height of the submersible blade $H = 1.4m$, blade chord length $c = 1.3m$, main angle of attack $\alpha = 18^o$, number of blades $N_{pal} = 5$.

Fig. 10 shows the torque $T_{r,i}$ developed by a single blade versus the positioning angle; the torque is computed by formula (4). Fig. 11 shows the total torque at the rotor shaft $T_{r\Sigma}$ developed by all blades versus the positioning angle. The total torque is given by formula (5). Fig. 12 shows the total torque $T_{r\Sigma}$ versus the positioning angle for three water flow velocities V_∞: 1 *m/s*, 1.3 *m/s* and 1.6 *m/s*.
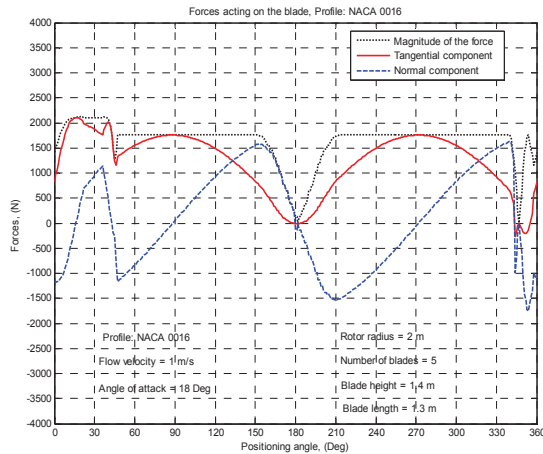
Figure 9: Magnitude, tangential component and normal component of the hydrodynamic force of a rotor blade versus the positioning angle.
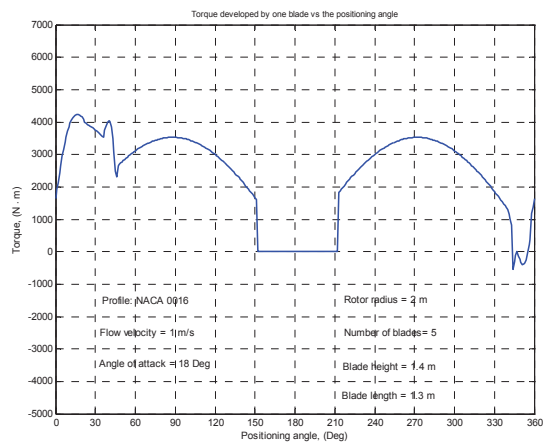

Figure 10: Torque $T_{r,i}$ developed by the rotor blade versus the positioning angle.
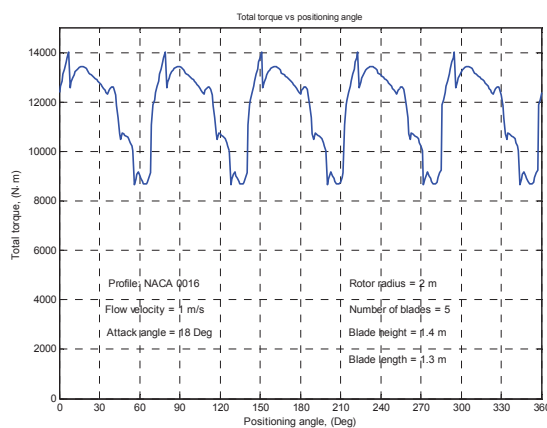

Figure 11: Total torque $T_{r\Sigma}$ developed by 5 blades at rotor shaft versus the positioning angle.

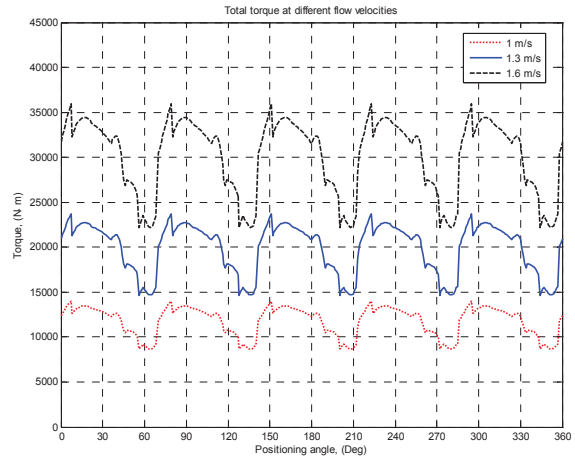The graph of the moment coefficient $C_{M,ref}$ versus the angle of attack α is shown in fig. 14.

Figure 12: Total torque $T_{r\Sigma}$ at rotor shaft versus the positioning angle for various water flow velocities.
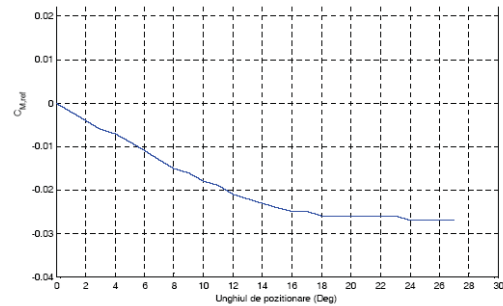

Figure 13: Moment coefficient $C_{M,ref}$ versus the angle of attack for NACA 0016 profile.

Taking into account the fact that the hydrodynamic force is not applied in the blade fixing point O' (see fig. 14), this force produces the so-called pitching moment. This moment is determined with respect to the reference point P situated at ¼ distance of the chord from the leading edge B.

Figure 14: Location of the blade fixing point.

For the angle of attack $\alpha = 18^o$ the moment coefficient $C_{M,ref} = -0.026$. Thus, from relation (56) results that $C_M = 0.0439$. The moment with respect to the reference point P is

$$M = \frac{1}{2} C_M \rho V_\infty^2 c S_p = -39.92 \ N \cdot m,$$

where $V_\infty = 1m/s$, $c = 1.3m$ and $H = 1.4m$. In $O'x'y'$ coordinate system, the components of hydrodynamic force are given by relation (3). Applying the previously obtained values F_L and F_D gives:

$$F_x = 1601.2 \ N, \ F_y = -413.8 \ N.$$

Then $\left| O'P \right| = \left| M \right| / \left| F_{x'} \right| = 0.0249 \ m \approx 25 \ mm.$

In order to ensure the stability of the blade motion, the fixing point W should be selected such that $25 \ mm \leq \left| O'W \right| \leq H$, where $H_{min} \leq H \leq H_{max}$. Values H_{min} and H_{max} are chosen in order to ensure that the friction force in the kinematical couples of the orientation mechanism is minimal.

To determine the optimal working angle of attack it is necessary to compute the value of the torque developed by one blade and the total torque for several values of the angle of attack, namely: $\alpha = 15^o$, 17°, 18°, 20°, (see fig. 15−16). In this context the angle of attack for the blade with hydrodynamic profile NACA 0016 was chosen $\alpha = 18^o$.
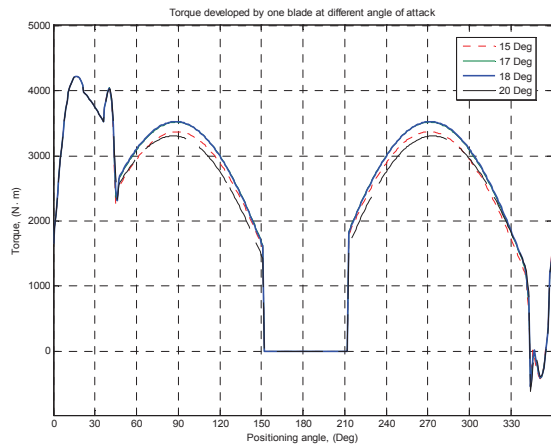

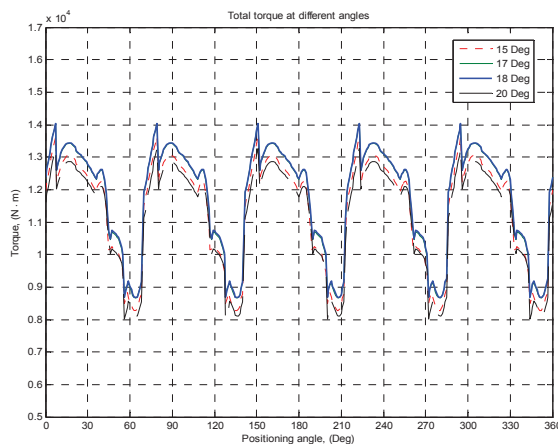Figure 15: Torque $T_{r,i}$ developed by one blade versus the positioning angle.

Figure 16: Total torque $T_{r\Sigma}$ developed by 5 blades versus the positioning angle.

Also, the performance of 3-, 4- and 5-blades rotor was analyzed. The total moment developed by the rotor shaft was computed and the results are presented in fig. 17.
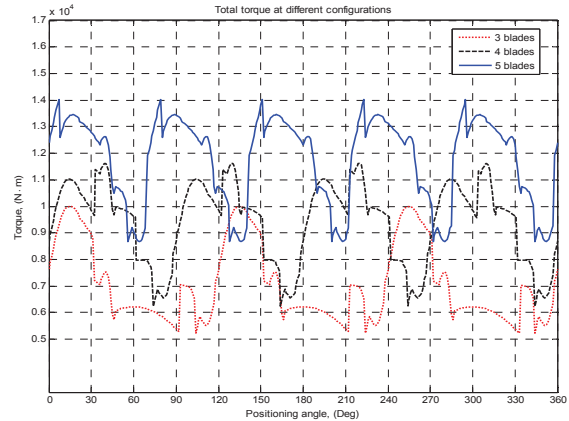

Figure 17: Total torque $T_{r\Sigma}$ developed at the 3-, 4- and 5-blade rotor shaft versus the positioning angle.

4. CONCLUSIONS

The hydraulic turbine with 5 hydrodynamic profile blades assures conversion of 49.5% of the energetic potential of water stream with velocity 1.3 m/s. The optimal orientation of the blades with respect to water stream direction (enabled by a guidance mechanism) assures participation of all blades (even those moving upstream) in generating the torque at the rotor shaft.

References

[1] I. Bostan, V. Dulgheru, V. Bostan, R. Ciuperca *Anthology of Inventions: Systems for Renewable Energy Conversion*, Technical University of Moldova, Chisinau, 2009.

[2] J. Moran, *An Introduction to Theoretical and Computational Aerodynamics*, John Wiley and sons, 1984.

[3] J. Katz, A. Plotkin, *Low Speed Aerodynamics, From Wing Theory to Panel Methods*, Mac-Graw Hill, 1991.

[4] G.K. Batcelor, *An Introduction to Fluid Dynamics*, Cambridge University Press, 1970.

[5] T. Cebeci, P. Bradshaw, *Momentum Transfer in Boundary layers*, Hemisphere Publishing Corportation, 1977.

[6] W.C. Reynolds, T. Cebeci, *Calculation of Turbulent Flows*, Springer-Verlag, Topics in Applied Physics Series, Vol.12, 1978.

[7] R.Michel, *Etude de la Transition sur les Profiles d'Ales*, Onera Report, 1/1578A, 1951.

[8] H.B. Squire, A.D. Young, *The Calculation of the Profile Drag of Aerofoils*, R.&M.1838, ARC Technical Report, London, 1938.